Soft Matter

PAPER

View Article Online
View Journal | View Issue

Cite this: *Soft Matter*, 2025, **21**, 7710

Surfactant-laden micro-scale droplet coalescence in Bancroft-breaking systems

Yun Chen, †[a] Negin Bahadori‡[b] and Cari S. Dutcher *[ac]

The dispersed droplets in liquid–liquid droplet emulsions are often stabilized by the surfactant molecules adsorbed onto the droplet interfaces, which reduces the interfacial tension and generally inhibits droplet coalescence. Other factors, such as viscous stress and Marangoni stress, will also have major impacts on droplet stability. In this paper, systematic droplet coalescence experiments will be presented using a microfluidic Stokes trap geometry, as a function of viscosity ratio between droplet and continuous phase as well as surfactant concentration. The results show that more coalescence can be observed for systems with a lower viscosity ratio (smaller than 1), while few coalescences are observed for a higher viscosity ratio (larger than 1), as expected. More surprisingly, a non-monotonic trend of film drainage time as a function of surfactant concentration is observed for both Triton X100 and Glucopon 225DK. The film drainage time first increases and then decreases followed by plateaus with the increase of surfactant concentration, until a critical concentration value is reached. To better understand the non-monotonic relationship between film drainage times and surfactant concentration, two Marangoni numbers defined based on (1) the ratio of Marangoni time scale with surfactant diffusion timescale, and (2) the ratio of Marangoni stress with interfacial tension, are examined. The results from both Marangoni scaling agree with the experimental observations.

Received 27th May 2024,
Accepted 11th August 2025

DOI: 10.1039/d4sm00644e

rsc.li/soft-matter-journal

Introduction

Droplet coalescence is often a critical step during the process of separation of liquid–liquid emulsions. Forming larger droplets through droplet coalescence is particularly useful when the dispersive phase droplet is microscale. In most cases, those microscale droplets are difficult to separate using simple gravity separators. The presence of unseparated microscale droplets may cause unwanted consequences and must be removed during the operation. For instance, bilgewater is oily wastewater (oil-in-water) that is found in the lower compartment of the ship.[1–4] Diesel oil usually appears as microscale droplets in the water due to the presence of detergents or grease on board. International Maritime Organization (IMO)[5] prohibited the direct offshore discharge of the bilgewater into seas if it contains more than 15 parts per million (ppm) of oil, as it may cause serious pollution to the environment. However, surface active molecules in the detergents or fuels can stabilize the oil droplets and prevent them from coalescing, which significantly increases the difficulty of removing those oils.

Similar circumstance of unwanted liquid dispersions also occurs in diesel fuel filtration systems.[6] During the transportation of diesel fuel, water can be entrained as micro-scale droplets in the fuel oil, which becomes water-in-oil emulsion.[7] The water droplets can damage diesel-powered equipment by causing rust or corrosion. These water droplets are usually stabilized by the surface-active additives present in the fuel, which inhibit the coalescence of droplets. Another situation of unwanted droplet emulsion can be involved is that fuel droplets may be found entrapped in the water in aqueous film forming foam (AFFF). AFFF is commonly used to extinguish a fuel pool fire,[8–11] which is usually spread as a layer of thin film over the fuel. Due to the presence of the foam stabilizer, or surfactant, some fuel droplets will form and suspend in the bulk of the aqueous phase of the foam. These droplets will remain in the liquid or the bubble walls, potentially disrupting the stability or lifetime of the foam. To better understand the stabilization or destabilization of these complex, surfactant-laden emulsion systems, it is first important to understand the mechanism of droplet stability.

Soluble surfactants can be initially present or mixed into one of the bulk phases with a given bulk concentration. Those

[a] *Department of Mechanical Engineering, University of Minnesota – Twin Cities, 111 Church Street SE, Minneapolis, MN 55455, USA. E-mail: cdutcher@umn.edu*
[b] *Department of Mechanical Engineering, Institute for Micromanufacturing, Louisiana Tech University, Ruston, LA, 71272, USA*
[c] *Department of Chemical Engineering and Materials Science, University of Minnesota – Twin Cities, 421 Washington Avenue SE, Minneapolis, MN 55455, USA*
† Current address: Mechanical Engineering, California State Polytechnic University, Pomona, Pomona, CA, 91768, USA.
‡ Current address: Chemical and Environmental Engineering, University of California, Riverside, Riverside, CA, 92507, USA.

surfactant molecules undergo several processes to transport to the liquid–liquid interface. First, the surfactant molecules in the bulk solution will migrate and diffuse to the region near the droplet interface, also known as the subsurface. Surfactant diffusion time depends strongly on bulk concentration, molecular diffusivity,[12] and depletion depth.[13] Following the diffusion process, the surfactant molecules in the subsurface region will then *adsorb* to or *desorb* from the interface due to the entropic driving force, causing the depletion of surfactants in the subsurface. The interfacial tension (IFT) of the droplet starts decreasing from its surfactant-free value, γ_0, as the surfactant molecules undergo adsorption to the interface. In general, the IFT reaches an equilibrium value, γ_{eq}, after some time, until the concentration of molecules on the interface becomes constant. Due to the simultaneous diffusion and adsorption processes during the surfactant transport, the timescale for the IFT to reach equilibrium value is strongly dependent on the surfactant transport rate, quantified as the timescale for the diffusion, τ_D, as mentioned earlier, and the timescale for adsorption, τ_{ads}. Comparing the magnitude between τ_D and τ_{ads}, the surfactant transport can be categorized as diffusion-limited and kinetic-limited. If $\tau_D \gg \tau_{ads}$, the surfactant transport is diffusion-limited, while for $\tau_D \ll \tau_{ads}$, surfactant transport is kinetic-limited. Based on the definition of the aforementioned timescales, a more well-defined dimensionless number $\Lambda = \Gamma^2(\beta C_\infty + \alpha)/C_\infty{}^2 D$, developed by Alvarez,[14] is able to indicate whether the surfactant transport is diffusion-limited or kinetic-limited, if $\Lambda \gg 1$ or $\Lambda \ll 1$, respectively. Here, Γ is the surface coverage of surfactants, C_∞ is the bulk phase surfactant concentration, D is the diffusivity of molecules, and β and α are the adsorption and desorption rate constants, respectively. Thus, the magnitude of τ_D compared to τ_{ads} is significant for the characterization of surfactant transport.

Beyond the impact of diffusivity and bulk concentration on τ_D, studies have also shown that the apparent timescale for diffusion can also be affected by the radius of the curvature,[6,15,16] and bulk convection.[17] For instance, in diffusion-limited surfactant transport, highly curved micrometer-sized droplets reach an equilibrium IFT significantly faster than large millimeter-sized droplets or planar interfaces, due to the reduced depletion depth.[13] Recent studies have also shown that the phase containing the surfactant (dispersed *versus* continuous) can also influence surfactant transport time scales[18] and equilibrium surface tension.[19,20] Particularly, an enhanced apparent surfactant diffusion rate can also be achieved by the implementation of the external convection[17] due to the decreased surfactant diffusion boundary layer for a convex spherical interface. In addition, surface tension for a concave interface can be higher than a convex interface[19] due to the depletion of the surfactant molecules in the bulk. Based on the aforementioned factors, a lower equilibrium IFT or shorter surfactant transport timescale decreases the ability for the droplet to coalesce and thus stabilizes the emulsions.

While studies on soluble surfactant transport onto the interface of a single droplet are important for understanding emulsion stability, it can be even more important to study the soluble surfactant transport and fluid motion behavior on the film between two interacting droplets. Here, when two droplets approach each other, a thin film forms and must drain for the droplets to coalesce. When the film drains, the shear stress at the fluid interface will drag the surfactant molecules away from the thin film region, which induces the surfactant concentration gradient along the interface. When the surfactant is in the continuous phase, the surfactant gradient that forms along the film interface will cause the Marangoni stress that is in the opposite direction to the drainage flow,[21] which inhibits the film drainage and increases the drainage time. Studies have suggested that this Marangoni stress can be suppressed when soluble surfactant molecules are present inside the droplets (dispersive phase).[3,21]

When the surfactant is inside the droplets, the molecules can diffuse and adsorb onto the thinning film during the drainage process. The repopulation of the surfactant molecules will diminish the surfactant gradient along the interface and weaken the Marangoni stress. In this case, the film drainage is no longer hindered, and the drainage time can be reduced. In addition to the impact of the Marangoni stress on the film drainage, interfacial mobility also plays an important role in the film drainage process.[22,23] The interfacial mobility is determined by the viscosity ratio between the dispersive and continuous phase, λ. For instance, if $\lambda \gg 1$, the higher viscous stress at the droplet interface can inhibit the film drainage, while for $\lambda \ll 1$, the film drainage is less affected by the viscous stress.[3,23] In practical applications, an o/w emulsion generally has a higher viscosity ratio than a w/o emulsion; therefore, the phase plays an important role in influencing interfacial mobility. Another factor that will affect the film drainage is the collision angles. The impact of collision angles has been investigated by several studies (Leal 2004,[24] Narayan *et al.* 2020[25]). In particular, the external hydrodynamic force will change its sign from positive to negative when the droplet rotates from 0° to over 45° such that the two droplets are pulled away from each other, which, under the right conditions, can induce dimpling at the interface and change the time it would take for coalescence relative to a head-on collision.

The coalescence of two droplets has been extensively studied by different groups, particularly focused on the film drainage and film rupture based on the collision of two droplets (Chesters 1991[26]). The study by Hu *et al.*[27] first defined the critical capillary number and found the scaling with droplet radius and viscosity ratio based on the polybutadiene drops in PDMS. In a following work by Yang *et al.*,[28] they defined a dimensionless drainage time that scales as $Ca^{3/2}$ particularly at higher values of *Ca*. A later study by Ha *et al.*[29] started looking into the impact of surface-active copolymer on droplet coalescence, which they found the copolymer will increase the film drainage time and thus inhibit the coalescence. The same study also shows that the film drainage time also increases when *Ca* increases due to the increased lateral extent of the thin film as a result of the deformation. The scaling of film drainage time *versus Ca* was then further studied by Hsu *et al.*,[30] in which they considered the impact of the droplet radius and the viscosity ratio. This seminal work studying film drainage established a

foundation for later research regarding film stability and droplet coalescence.

In general, the fundamental basics of droplet coalescence and film drainage have been well-established both theoretically and experimentally. Seminal studies on droplet coalescence include the scaling of film drainage time with capillary number,[31,32] the mechanism of the Marangoni stress and mobility,[21–23,33] and the hydrodynamic conditions for deterministic *versus* stochastic thin liquid film rupture.[34,35] Particularly, Kumar[36] has developed computer-controlled microfluidic devices to manipulate two soft particles in a 2D viscous flow, which has been widely employed in studying droplet coalescence and particle interactions. However, although previous experimental work has focused on micro-scale droplets with insoluble surfactants, most of those studies focused on the systems that follow the Bancroft rule, where the surfactants are soluble in the continuous phase. Seminal studies[37,38] have performed experiments with surfactants in the continuous phase or nanoparticles in the droplet phase to investigate droplet formation behavior in microfluidics, but these studies only consider surfactants in the continuous phase. Numerical works[39–41] were also performed to study the interfacial flow in the presence of surfactants in the droplet phase, but these works do not have further experimental validations. However, there still remains the need for experimental study on the droplet coalescence. The theoretical work based on the Marangoni stress and mobility in film drainage has been well studied, but few of the works have systematically investigated the impact of these two factors on film drainage with the presence of surfactants *via* experiments. Quantification of the film drainage time for the surfactant concentration will provide key insight into the improvement strategies for emulsion stability control and water treatment.

The goal of this work is to experimentally study the impact of surfactant concentration and viscosity ratio on the film drainage time of microscale droplets in the presence of soluble surfactants both inside, and outside, the dispersed droplet phase. Film drainage times for systems with different surface concentrations in the droplet phase, leading to different Marangoni stresses, as well as varied viscosity ratios, λ, leading to different viscous stresses at the interface are investigated to further understand the mobility impact on the droplet coalescence. Finally, scaling analysis is performed to provide a possible explanation of a non-monotonic trend observed in film drainage time when surfactants are present inside the droplet phase.

Materials and methods

Microfluidic devices are used to perform the Stokes trap experiments as shown in Fig. 1 and 2. To make the devices, the silicon wafers are first fabricated with a patterned mask using soft lithography techniques in the clean room with SEUX sheets. Poly-dimethylsiloxane (PDMS, Sylgard 184, Dow) is poured on the master wafer and cured at 70 °C in the oven overnight. The cured PDMS device is then cut, and holes are punched at the injection ports with a 1.5 mm biopsy punch.

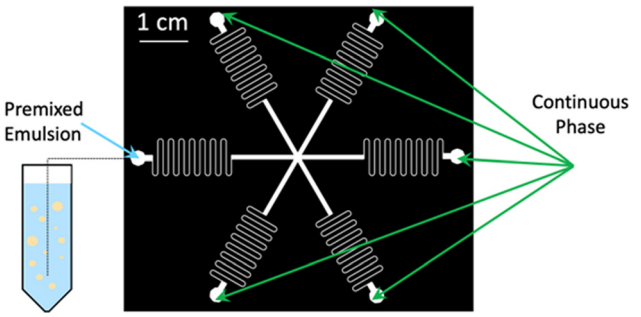

Fig. 1 The 6-channel Stokes trap device contains 6 inlets with the cross-slot in the center. The height of the channel is 120 μm, and the channel width at the cross-slot is 400 μm. Each inlet is connected to the serpentine channel that is used to reduce the flow speed. The emulsions are premixed in a centrifuge vial and injected through the left side of the device. The continuous phase is then injected through all the other five channels.

The device is then bonded with a PDMS-coated glass slide after plasma treatment (Harrick Plasma). For water-in-oil systems, the device, after being baked in the oven for 4 hours, is treated with NOVEC 1720 (3M) to make the PDMS more hydrophobic. The device is left overnight to let the NOVEC 1720 evaporate and then baked at 130 °C for 30 min. The treated device is then soaked in oil overnight before it is used for experiments.

The liquids used in the experiments are prepared and stored in the centrifuge tube as a fluidic reservoir and injected into the devices using Teflon tubing (1/16″ OD, 0.02″ ID, IDEX Health and Science) that is connected to a PEEKsil tubing (1/16′ OD, 100 μm ID, IDEX Health and Science) with Delrin Union connectors (1/4-28 port, IDEX Health and Science). The PEEKsil tubing is inserted into the injection ports of the devices. The liquid in the centrifuge tube is pressurized using pressure regulators (QPV series, Proportion-Air) that are controlled by signals from the National Instruments Data Acquisition (DAQ) board (cDAQ-9174 chassis, NI 9264 AO, NI 9201 AI) with a LabView program.

Microfluidic experiments

Two different designs of the devices were used. Fig. 1 shows the 6-channel Stokes trap device with the serpentine channel. For this design, the emulsion is first pre-mixed in a centrifuge vial and then injected into one of the inlets through the tube. The continuous-phase liquid is then injected into the other five inlets. By changing the pressure in each inlet, the device is able to generate various types of flow patterns such that it can trap two different droplets. This allows the flow to trap and hold droplets for up to 1 hour to observe the coalescence of droplets within the given time. In the current 6-channel experiment, the droplets may flow at different channel depths. For the droplets in contact, only those that appear at the same focal plane will be considered to observe the coalescence possibility. The purpose of using this device is to qualitatively observe the interaction of droplets with a variety of sizes, velocities, and liquid–liquid systems to simulate emulsions in a practical environment. Fig. 2 shows image sequences of one droplet (labeled 1) approaching the other droplet (labeled 2) in the

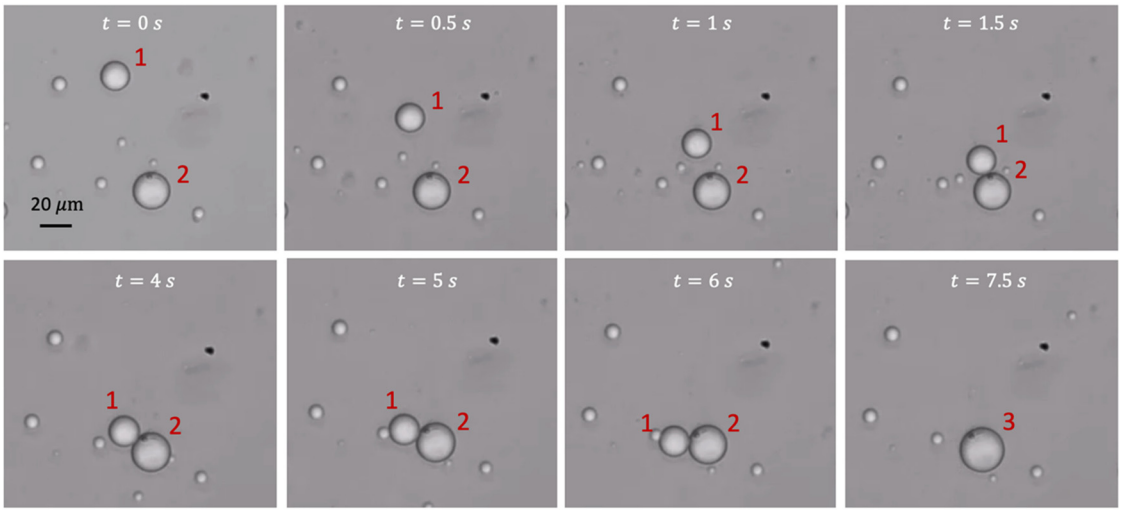

Fig. 2 Image sequences of droplet 1 approaching the trapped droplet 2 in the cross-slot of the 6-channel Stokes trap device and finally coalesces to form droplet 3.

cross-slot of the 6-channel Stokes trap device. A stagnation point is generated at the cross-slot based on the flow field controlled by the pressure regulators. Droplet 2 is held stationary at the stagnation point while droplet 1 is moving toward droplet 2 driven by the external flow. This stagnation point can be adjusted and move the trapped droplet 2 to a desired location using LabView program, allowing droplet 1 to collide with droplet 2 precisely. When touching droplet 2, droplet 1 rotates and eventually coalesces with droplet 2 and forms droplet 3. Those small droplets shown in Fig. 2 are generally attached to the bottom of the channel with size smaller than 10% of the channel height. Given the Reynolds number of the system Re $\sim 4 \times 10^{-4}$, the impact of those small droplets on the experimental results is anticipated to be minimized.

A second design of the microfluidics device is the 4-channel Stokes trap device with the T-junction as shown in Fig. 3. In this design, one liquid is injected through 4 of the injection ports as a continuous phase, while the other liquid is injected as the dispersive phase. Droplets of certain sizes are first formed at the T-junction and flow downstream to the cross-slot. This allows the coalescence experiments with on-site generation of droplets with consistent sizes, which provides better observation of interaction between individual droplets. By controlling the pressure from each port of the continuous phase, the droplet at the cross-slot can be steered to the stagnation point and trapped in the cross-slot with adjustment of the flow rate. The 4-channel study is specifically designed to control droplet size allowing for consistent assessment of surfactant concentration effects,[42,43] while the 6-channel experiments used droplet size variability to explore scenarios more closely resemble real-world emulsions. The dual-approach design enables our work to bridge the gap between idealized systems and practical applications.

The channel length of the 6-channel and 4-channel microfluidics devices is adjustable based on the input pressure of the flow. In both cases, the channel height is 120 μm, and the channel width is 400 μm. For both designs, the pressure from each inlet of the continuous phase is manipulated using a customized LabView program. This flow control strategy uses a Model Predictive Control (MPC) algorithm implemented using Automatic Control and Dynamic Optimization (ACADO) and was developed by Kumar[36] and Shenoy *et al.*[44–46] Once a droplet is trapped, it can interact with the following incoming droplets, and their coalescence can be studied.

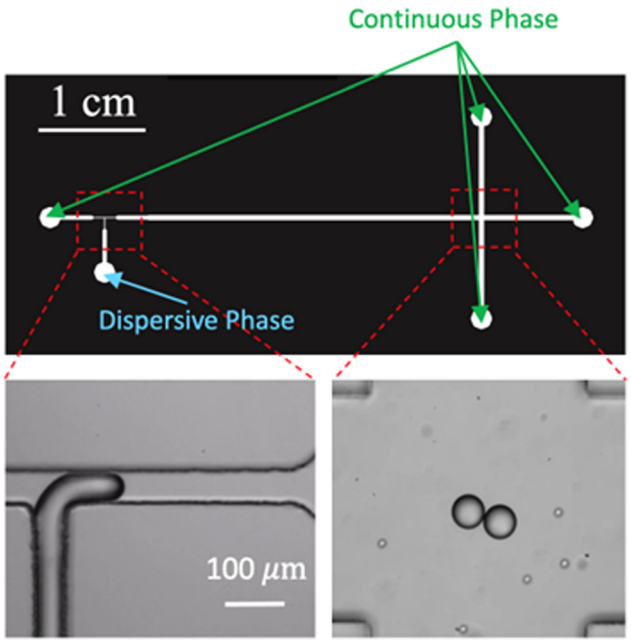

Fig. 3 (Top) A microfluidic Stokes trap device is used for coalescence experiments. The height of the channel is 120 μm, and the channel width at the cross-slot is 400 μm. One liquid is injected into the 4 ports as a continuous phase and another liquid is injected as the dispersive phase. (Bottom Left) The droplets are generated at the T-junction. (Bottom Right) Droplets are trapped at the stagnation point of the cross-slot and interact with the following droplets. Note that the bottom images are of only a sub-portion of the region indicated by the red dashed boxes.

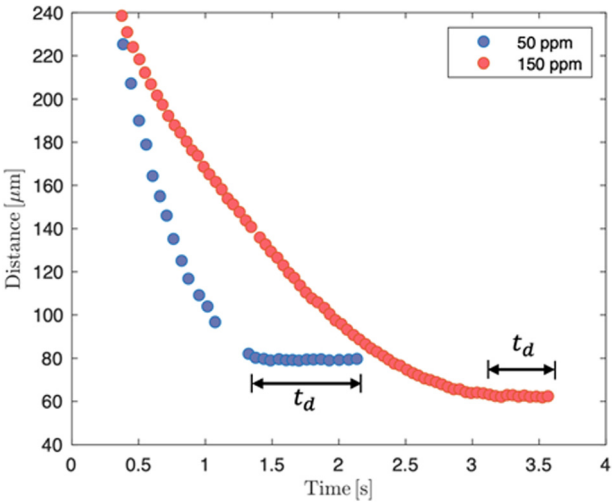

Fig. 4 The center-to-center distance between the droplets as a function of time for Triton X-100 in water (water-in-LMO) of two concentrations. The plateau of the curve is defined as the film drainage time, t_d.

The droplet coalescence is visualized and recorded using a Basler ace acA1300-60gm camera at a frame rate of 30 fps (~33 ms each frame). Particularly, the videos recorded from the 4-channel device are processed using a customized MATLAB code to track the droplets. A particle tracking approach by Crocker *et al.*[47] is also implemented as a function in the image processing code, which is used to select the desired droplets to measure the droplet film drainage time. The position, size, velocity, and strain rate of each droplet are measured from the videos. When two droplets are moving toward each other in the video, the center-to-center distance between them is calculated and plotted as a function of time as shown in Fig. 4. As the droplets move closer, the distance curve becomes a plateau once it decreases to 2R, indicating the center-to-center distance now becomes constant with only changes in the thin film less than the resolution of an optical microscope. As the distance between them eventually reaches a plateau, and the time scale of this plateau is defined as the time for the film drainage between the two droplets. Based on the measurement of the approaching droplet velocity u and location x, the strain rate $G = \frac{\partial u}{\partial x}$ can be extracted from the experiments (Narayan *et al.* 2020[25]). In particular, the measured velocity u as a function of time t, can be fitted by an exponential function, $u = ae^{bt}$, where a and b are two fitting parameters. By the chain rule, $\frac{\partial u}{\partial x} = \frac{\partial u}{\partial t}\frac{\partial t}{\partial x}$, while, $\frac{\partial u}{\partial t} = abe^{bt}$, and, $\frac{\partial t}{\partial x} = \frac{1}{u}$, such that the strain rate $G = b$.

Table 1 Systems studied in the experiments

Continuous phase	Dispersive phase	Surfactant (water soluble)
Light mineral oil	Water	Triton X-100
Light mineral oil	Water	Glucopon 225 DK
Water	Heptane	Glucopon 225 DK
Water	Heptane	Dow 502 W
Water	Hexadecane	n/a

Chemicals and materials

In the 6-channel microfluidics design, heptane (Chem-Products, 99%, density = 0.67 g cm^3, viscosity = 0.38 mPa s) and hexadecane (Sigma–Aldrich, 99%, density = 0.76 g cm^3, viscosity = 3.45 mPa s) are used as dispersive phase, while water is used as the continuous phase. These two systems are applied to investigate the fuel droplets entrapped in the liquid phase, particularly in firefighting foams. In the 4-channel design, light mineral oil (Sigma–Aldrich, density = 0.83 g cm^3, viscosity = 26.8 mPa s) is used as the continuous phase liquid and distilled water as the dispersive phase. In general, mineral oil is a complex mixture of refined saturated hydrocarbons derived from petroleum,[48] consisting of straight-chain alkanes, branched isoalkanes, and ring-structured cycloalkanes.[49] Light mineral oil (LMO) is usually composed of isoalkanes and cycloalkanes with carbon numbers from 15–25.[49] Mineral oil has been shown to be used as a model liquid for the oil phase to study a variety of systems such as the oil filtration system,[3,25,50] bilgewater treatment,[2,4] protein synthesis,[51] and polymerase chain reaction (PCR)[52–54] for diagnosis of infectious diseases like coronavirus. The measured surfactant-free IFT of LMO-water, hexadecane-water, and heptane-water used in this study are 47 mN m^{-1}, 53 mN m^{-1}, and 52 mN m^{-1}, respectively.

Three water-soluble surfactants, Triton X-100, Glucopon 225 DK, and Dow 502 W are investigated in the current study (see Table 1). The chemical structures of the three surfactants studied are shown in Fig. 5. Here, Triton X-100 is a non-ionic surfactant with a hydrophilic polyethylene oxide chain and an aromatic hydrocarbon hydrophobic group, with 99% concentration in water (Sigma–Aldrich, density = 1.06 g cm^3), with the formula C_8H_{17}–C_6H_4–$(OCH_2CH_2)_n$–OH, where n represents the number of ethylene oxide (EO) around 9.5 in average.[55] Glucopon 225DK is an alkyl polyglycoside that contains C_8–C_{10} alkyl chains attached to short chains of glucose units,[56] which is a 68–72% by weight concentrate in water (Contributed by BASF Corporation, density = 1.13 g cm^3).[57] Dow 502W is a silicone

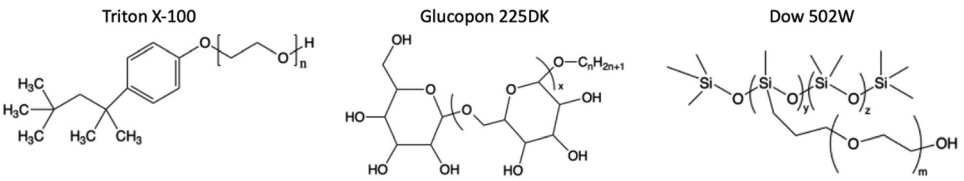

Fig. 5 Structures of surfactant components in Triton X-100, Glucopon, and Dow Corning 502W.

polyether copolymer with 100% by weight concentrate in water (Contributed by Dow Corning Co., Midland, MI, density = 0.97 g cm^3).[57] Both Glucopon 225DK and Dow 502W are generally used in the foam generation for AFFF. The IFT of the interface between the two liquids studied here with surfactant added is measured using a drop shape analyzer (Krüss DSA 30).[6,18]

Experimental results

Characterization of surfactants

The surfactants used in the current systems are first characterized by measuring the dynamic interfacial tension using a pendant drop. The maximum surface concentration, equilibrium constant, diffusivity, and adsorption rate constant are obtained to understand the surfactant transport behavior. Fig. 6 shows the equilibrium interfacial tension, γ_{eq}, as a function of concentration for both Triton X-100 and Glucopon 225 DK added to water for water/LMO systems. Based on the measurement, the Triton X-100 has a much lower IFT comparable to that of the Glucopon 225 DK. The critical micelle concentration (CMC) was determined based on the abrupt change of slope of the IFT curve as shown in Fig. 6. As IFT becomes constant after reaching CMC, the slope of the IFT curve plateaus or significantly reduces. The point at which the slope changes is usually suggested as the CMC of the surfactant. CMC of Triton X-100 observed from our measurement is consistent with the measurement from Church *et al.*,[4] 324 ppm, as shown in Fig. 6. According to the measurement, the CMC of Glucopon 225 DK is approximated at about 1000 ppm. In addition, beyond this concentration, a color change in the solution was observed. The values in Fig. 6 are used to extract the surfactant maximum surface concentration, Γ_∞, and equilibrium constant, κ. The measured dynamic IFT for both surfactants in various liquid–liquid systems is included in the SI. Here, Γ_∞ indicates the maximum coverage of the surfactant can be absorbed onto an interface, and $\kappa = k_{ads}/k_{des}$ represents the affinity of surfactant to the interface, where k_{ads} and k_{des} are adsorption and desorption rate constants. κ can be extracted using Langmuir isotherm and equation of state,[3,12,18] $\Gamma_{eq} = \Gamma_\infty \kappa C/(1+\kappa C)$, where Γ_{eq} is the equilibrium surface coverage and C is the bulk concentration. In addition, the diffusivity of both surfactants will be obtained by fitting the long-time limited Ward and Tordai equation[12,18,58,59] to the dynamic IFT from pendant drop measurements. While the Ward and Tordai equation assumes the diffusion of a single species of surfactant, it has been used as an effective framework for estimating dynamic adsorption properties of commercial surfactant mixtures. Therefore, a pseudo-single-component approximation is adopted for each surfactant in Ward-Tordai equation to evaluate the overall behavior of the surfactants in the current study.

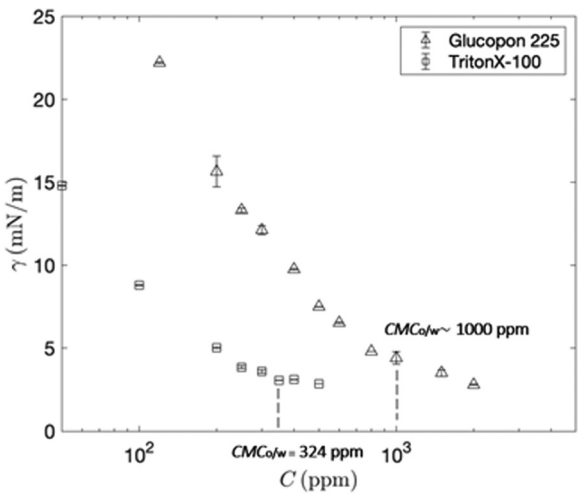

Fig. 6 IFT plotted as a function of surfactant concentration with both Triton X-100 (at equilibrium) and Glucopon 225 DK (at 10^3 s, near equilibrium) for the LMO-in-water system. Error bars from replicates. CMC of each surfactants for oil–water emulsions are indicated.

Table 2 shows the resulting extracted values for surfactant properties of both Triton X-100 and Glucopon 225 DK in various liquid–liquid systems. The fitted values of Triton X-100 are similar to those of Church *et al.*,[4] with slight differences explained due to the additional measured data near CMC as shown in Fig. 6 that leads to updated characterized values. The Γ_∞ of Glucopon 225 Dk is slightly larger than that of the Triton X-100, indicating that there are more numbers of Glucopon 225 surfactants covered at the interface of the droplets. κ of Triton X-100 is much higher than that of Glucopon 225 DK, suggesting that the surfactant molecules of Triton X-100 are more likely to be absorbed onto the interface. From the dynamic IFT measurement using pendant drop for both surfactants, the diffusivity of Triton X-100 is two orders greater than that of the Glucopon 225 DK, which means its molecules diffuse faster from the bulk to the subsurface of the droplet for millimeter scale. However, according to Liu, Rahti, *et al.* JCIS 2025, as a multi compound surfactant solution, the diffusivity Glucopon 225 DK extracted from the IFT measurement might be an ''effective'' diffusivity of the mixture, which could be lower than the expected ''actual'' diffusivity of the surfactant. In addition, the actual active ingredients of commercial Glucopon are less than 100%, so when the product is used as received, the value determined from adsorption data would result in lower-than-expected value than based on the pure surfactant alone. In addition, given the low diffusivity for the Glucopon systems, it is possible that kinetic-limitations may be at play. In that case, the Ward and Tordai model would not be applicable, as the model assumes

Table 2 Surfactant properties

Surfactant	Oil phase	M_w (g mol)	Γ_∞ (mol m^2)	κ (m^3 mol)	D (m^2 s)
Triton X-100	LMO	625	$(2.6 \pm 0.2) \times 10^{-6}$	1902 ± 824	$(2.05 \pm 0.49) \times 10^{-11}$
Glucopon 225 DK	LMO	424.2	$(3.7 \pm 0.7) \times 10^{-6}$	50 ± 34	$(2.04 \pm 1.8) \times 10^{-13}$

diffusion-limited transport. The resultant impact of the higher repopulation rate will be further discussed in the later sections. The values calculated in Table 2 use the Langmuir isotherm model and Ward and Tordai equation in the limit of long-timescale and no curvature effect, based on the fitted equations shown in Fig. S1 and S2. Additional characterization has also been performed using Ward and Tordai equation with curvature effect and Frumkin isotherm model, which are shown in Tables S1 and S2, respectively, in the SI.

Impact of viscosity ratio on droplet coalescence

Oil-in-water systems are being performed in the 6-channel Stokes trap device. Two different types of oil are used: hexadecane and heptane. As mentioned in the earlier sections, the purpose of using these two types of oil is to achieve two values of viscosity ratio between dispersive and continuous phase, $\lambda = \mu_d/\mu_c$. Here, λ = 3.45 and 0.38 for oil using hexadecane and heptane, respectively. In addition, a water-in-oil system is used in the 4-channel Stokes trap experiments such that λ = 0.038. Seminal studies[3,23] have shown the theoretical work of the influence of viscous ratio on film drainage. For instance, if $\mu_d \gg \mu_c$, or $\lambda \gg 1$, the viscous stress at the droplet interface strongly inhibits the drainage of the thin film between the droplets. On the other hand, if $\mu_d \ll \mu_c$, or $\lambda \ll 1$, there is less stress at the droplet interface to affect the thin film drainage.

Fig. 7 shows the phase diagram of droplet coalescence *versus* no coalescence based on viscosity ratio, λ and concentration of Glucopon 225 DK. As shown in Fig. 7, when λ = 3.45, no coalescence is observed even with no or low surfactants added in water within 1 hour. On the other hand, in the case of heptane in water when λ = 0.38, coalescence is observed with surfactants in water. In addition, for λ = 0.38, the coalescence is observed even with a much higher concentration of Glucopon 225 added to the water. This result clearly shows that when $\lambda < 1$, coalescence is likely to be observed due to the less impact of the viscous stress, which agrees with the previous work. In addition to the impact of the viscosity ratio, the surfactant concentration is also investigated here. At a viscosity ratio of λ = 0.38, coalescence is observed at 1 and 5 ppm; however, concentrations above 10 ppm do not lead to coalescence. Despite the fact that the viscosity ratio affects the droplet coalescence, the results here suggest that the concentration of the surfactants must also have an impact on the droplet coalescence. The data points in the gray region did not show coalescence based on our current experiments, but the boundary between coalescence and no coalescence is considered qualitative and may present a gradual transition instead of an abrupt change. In addition, other factors, such as internal flow inside droplet, may also play a role in affecting the film drainage and coalescence,[60,61] but this is beyond the current scope of study. We have included Figure S8 that is plotted based on the results in Fig. 7 with colormap of the capillary number. The capillary number of this set of experiments varies from Ca $\sim 10^{-6}$–10^{-4}.

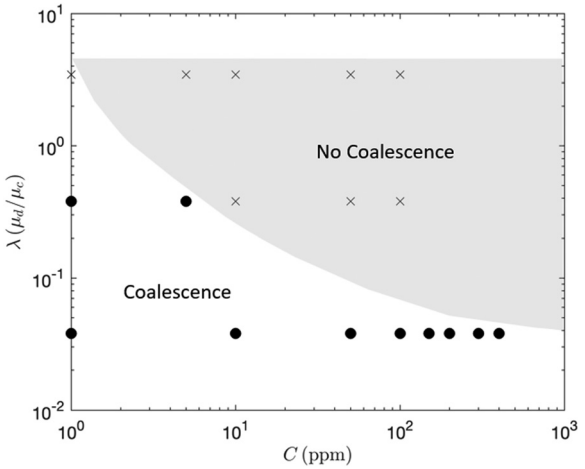

Fig. 7 Phase diagram showing the droplet coalescence dependent on both the viscosity ratio (λ) and concentration (C) of Glucopon 225 DK.

In the current study, we do observe a variation in collision angles between the droplets. However, the purpose of this section is to qualitatively observe the coalescence possibility based on a certain viscosity ratio rather than measuring the film drainage time. For the systems in which we do not observe coalescence, we were able to hold the two droplets together for up to 1 hour by controlling the flow patterns in the 6-channel device, regardless of whether the initial contact was glancing or not. The average coalescence time, droplet radius, and impact velocity from both 6-channel Stokes (Fig. 1) and 4-channel Stokes (Fig. 3) experiments are listed in Table 3. The various droplet radius and impact velocities from the experiments can be applied to a variety of real applications where external hydrodynamic flow, and the mixture of different compositions are involved. Despite those complications, while there are not sufficient data points to resolve the phase boundaries reliably, the results from Fig. 7 still qualitatively convey the general impact of viscosity ratio and concentration on droplet coalescence. Motivated by this result, a quantitative and systematic study of various concentrations of surfactants is presented in the next section.

Table 3 Droplet coalescence based on different viscosity ratio

Continuous phase	Droplet phase	$\lambda = \mu_d/\mu_c$	Surfactant + phase	Coalescence time (s)	Drop Radius Range (μm)	Ave impact velocity (μm s^{-1})
Water	Hexadecane	3.45	No surfactant	n/a	5–30	13.3
Water	Heptane	0.38	No surfactant	0.7–1.8	5–30	20.9
Water	Heptane	0.38	Glucopon 225 DK in water	1.5–6.2	5–30	28.6
Water	Heptane	0.38	Dow 502W in water	1.1	5–30	15.4
LMO	Water	0.038	Glucopon 225 in water	0.03–1.4	30–45	40

Impact of surfactant concentration on droplet coalescence

To understand the impact of the surfactant concentration on the droplet coalescence, the film drainage time has been determined from the coalescence experiments with varied surfactant concentrations using the 4-channel Stokes trap device. Droplets with radii ranging from 20–55 μm and strain rates from 5–55 s^{-1} were used in the experiments. Water-in-LMO system is studied, and the surfactants are added to the water phase (droplet phase). Fig. 8 shows the extracted film drainage time, t_d, *versus* surfactant concentration for both surfactants, based on the methods described in the Materials and Methods section. In the SI, the results in Fig. 8 are replotted with a color map based on droplet velocity (Fig. S4), radius (Fig. S5), and strain rate (Fig. S6), with the range of these values used in the experiments given in the labeled color bars.

Fig. 8(a) shows the film drainage time for Triton X-100 inside the droplets. The trend of the measured t_d can be interpreted based on the concentration in the regions either below or above CMC (~324 ppm[4]). The error bars in the figures indicate the standard deviation of the film drainage times obtained from approximately 5 repetitive experiments for each concentration. For the Triton X-100 below CMC, when the surfactant concentration is increased from 0 to 50 ppm (blue shade region), the film drainage time increases dramatically. As expected, the decrease in IFT inhibits the droplet coalescence. Interestingly, the film drainage time then decreases when the concentration of Triton X-100 increases from 50 to 300 ppm (white region). This inverse trend suggests that increasing the surfactant concentration can enhance the film drainage and destabilize the droplets in the current system. When the surfactant concentration is further increased above CMC, t_d plateaus and starts showing scattered values (gray shade region). The non-monotonic results here are different from what is expected. When the surfactant concentration increases, IFT decreases, and the resultant Marangoni stress becomes stronger.[3,21] In this scenario, it is expected that it should take a longer time for the film to drain before the droplets coalesce. The schematics of the interfacial flow behavior and interfacial deformation of the droplets can be referenced from Fig. 2 and Fig. 10 in Dai and Leal 2008.[62]

Similar results are observed for Glucopon 225DK as shown in Fig. 8(b). Here, t_d first shows a sharp increase from nearly 0s to 1s when 10 ppm is added (blue shade region). Following that, t_d starts decreasing when the concentration increases to 300 ppm (white region). Further increasing the concentration above 400 ppm, similarly, t_d plateaus and shows a large variation (gray region). The nonmonotonic results for both surfactants observed here are also different from what was reported by Narayan *et al.*,[25] in which the film drainage time increases monotonically with the concentration of SPAN 80. However, in the work by Narayan *et al.*,[25] the surfactant SPAN 80 is added to the continuous phase (outside droplet), while the surfactant in the current study is added to the dispersive phase (inside droplet). The measured film drainage time for both surfactants is also presented as Box and Whisker plot to visualize the data distribution and statistics as Fig. S3 in SI. Note that the wall confinement may also contribute to the scattering of the measured film drainage due to the possible droplet deformation and redistribution of surfactants.

The discrepancy between the current study and the work from Narayan *et al.* can be explained by the well-studied theory from seminal studies.[3,21] When two droplets are moving towards each other, a film forms in between the two droplets and the flow drives away the surfactant molecules from this region. The migration of the surfactant molecules results in the gradient of surfactant concentration at the interface of the droplets, which causes the Marangoni stress that is in the opposite direction of the film drainage. Particularly, with higher surface coverage, more surfactant molecules will be advected away from the film towards the stagnation point of the droplet interface. This will cause increased local surfactant concentration at the stagnation point as compared to the film region, which leads to a higher surfactant concentration gradient along the droplet interface. The Marangoni stress inhibits the flow of the film drainage, and therefore, stabilizes the droplet emulsion. Higher bulk

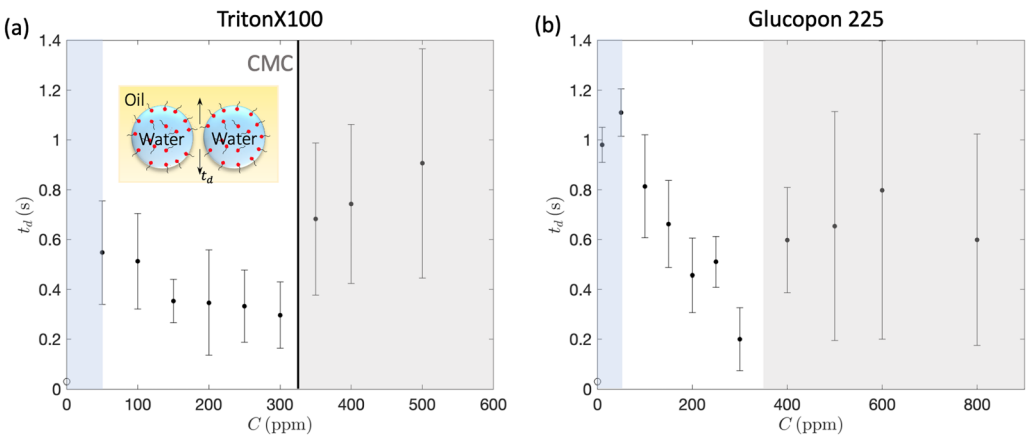

Fig. 8 (a) Film drainage time, t_d, between droplets with Triton X-100 in water for the water-in-LMO system. t_d first increases drastically from 0 s when surfactant concentration increases from 0 to 50 ppm. Further increasing of concentration decreases t_d, which then plateaus and shows large variation when concentration is above CMC. (b) Film drainage time, t_d, between droplets with Glucopon 225 DK in water for a water-in-LMO system.

concentration outside the droplets leads to a higher surface coverage. In this line of thought, increasing the surfactant concentration is expected to increase the film drainage time. Nevertheless, seminal work has shown that,[21] if the surfactant is added inside the droplet, the surfactant molecules will be able to repopulate and adsorb onto the depletion region of the interface during the film drainage, unaffected by the film flow. Those repopulated surfactant molecules suppress the concentration gradient and mitigate the Marangoni stress, such that the film drainage recovers to its flow rate with no surfactants. One possible explanation is that when the surfactant is inside, there is a recirculation flow that enhances the transport and adsorption of the surfactant onto the depletion region of the droplet interface. When the surfactant is outside, however, the draining film will push the surfactant in bulk away from the depletion region and inhibit its adsorption. This mechanism explains when surfactant concentration is increased, t_d first increases and then decreases for both Triton X-100 and Glucopon 225DK. The onset of Marangoni stress can also contribute to the initial sharp increase of the t_d when C is increased from 0 ppm to a certain value for both Triton X-100 and Glucopon 225. This initiation of Marangoni stress inhibits film drainage before the repopulation of surfactant can suppress it.

When further increasing the surfactant beyond a critical concentration, $\tilde{c}$, the film drainage time, t_d, for both surfactant plateaus and shows scattered values. For Triton X-100, the critical concentration $\tilde{c} \sim$ CMC. A possible reason is that when the bulk surfactant concentration reaches CMC, the monomer surfactant concentration saturates and the concentration gradient driving the surfactants to the interface and suppressing the Marangoni stresses is not enhanced with increasing concentration. and the Marangoni stress can no longer be suppressed, which prevents t_d from reducing further. When surfactant concentration in the bulk reaches at or above CMC, the surface coverage reaches its maximum value and saturates at equilibrium. However, two different situations may still cause disturbances in the concentration at the interface: First, when two droplets are in contact with each other, the surface convection due to film drainage will lead to an increase in local surface concentration that is higher than the maximum surface concentration. This, as a result, will cause fast desorption of surfactant back to the bulk leading to local depletion of surfactants (Stebe *et al.* 1991,[63] King and Leighton 2001[64]). A second situation is due to the droplet deformation and surface fluctuation during the film thinning process, which leads to the local compression and expansion of surfactant coverage as a result of bending and dilation of surface area. This will also cause the adsorption and desorption behavior of surfactant at the droplet interface which leads to surfactant concentration gradient. Therefore, it is still possible to observe surface concentration gradient with bulk concentration at or above CMC. These two situations may both cause the large scattering of film drainage time for concentrations above CMC. However, for Glucopon 225DK, $\tilde{c} \sim$ 400 ppm, which is, unlike that of the Triton X-100, well below the CMC of Glucopon 225. One possible reason is that there will be a sufficient amount of surfactants available inside the droplets to reach lower IFT and inhibit the droplet coalescence, as shown by the studies from Li *et al.*[19] and Kairaliyeva *et al.*[20] The plateau of t_d and the large variation for both surfactants will be explained using scaling analysis in the Discussion section.

To rationalize the relation between the film drainage time and various parameters, the dimensionless film drainage time is defined as $t_d^* = t_d\gamma/\mu_c R$, where γ is the equilibrium IFT, μ_c is the continuous phase viscosity, and R is the mean radius of the two droplets. Here, the mean radius $R = R_1R_2/(R_1 + R_2)$. R_1 and R_2 are the radius of the two approaching droplets that can be measured from the experiments. The capillary number is then defined as $Ca = \mu_c GR/\gamma$, which is to describe the ratio between the viscous force and interfacial tension. G is the strain rate of the incoming droplet and can be obtained from the extracted velocity as a function of time. t_d^* is plotted as a function of Ca for both Triton X-100 and Glucopon 225 DK as shown in Fig. 9. For both surfactants, the values of Ca are all within the order of 10^{-3} in the current experiments. When the Ca is smaller than 10^{-3}, t_d^* shows large variation with higher values. When further increasing the values of Ca to the order of 10^{-3}, t_d^* starts decreasing and

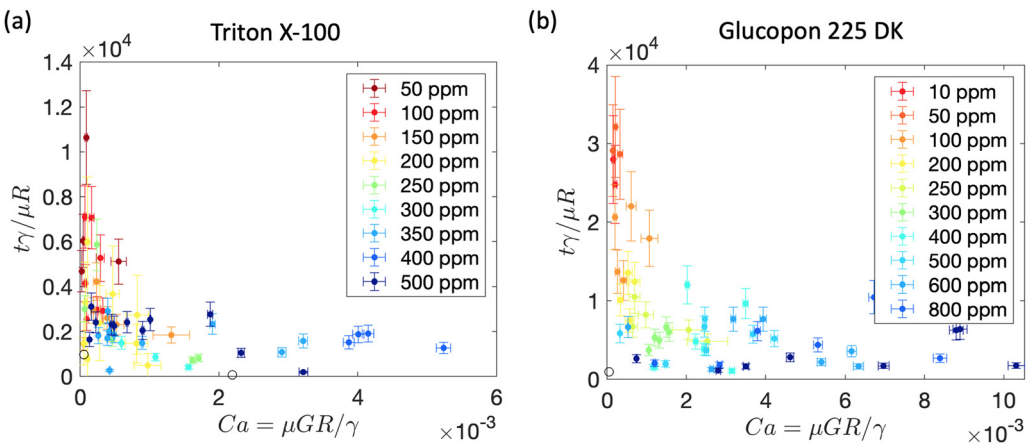

Fig. 9 The film drainage time is nondimensionalized as $t^* = t\gamma/\mu R$, and plotted as a function of $Ca = \mu GR/\gamma$ for (a) Triton X-100 and (b) Glucopon 225DK for various surfactant concentration. In both cases, when Ca increases, the dimensionless drainage time decreases and converges.

converges for both surfactants. The similar behavior observed for both surfactants suggests that, the dimensionless drainage time, t_d^*, must have a substantial relation to *Ca* regardless of the surfactant type and concentration. In general, higher *Ca* leads to smaller t_d^*, which destabilizes the droplets. Lower *Ca* increases t_d^*, though with a greater amount of experimental scatter, and stabilizes the droplets. As the change of *Ca* has impact on the film drainage behavior, Fig. 9 is also plotted using the color map showing the values of *Ca* in Fig. S9.

Discussion

Marangoni *versus* diffusion timescale: repopulation of surfactant to the interface

To quantitatively understand the transportation of surfactant molecules along the droplet interface, it is usually useful to investigate the Marangoni number, Ma. There are several ways to define Ma, as carefully reviewed by Manikantan & Squires.[65] Here, two Ma definitions perhaps particularly applicable to coalescence are explored to aid in the understanding of the film drainage time results. The first Ma examined is:

$$\mathrm{Ma} = \frac{\tau_D}{\tau_m} \tag{1}$$

where τ_D is the time scale for the surfactant diffusion to the droplet interface, τ_m is the timescale to establish the Marangoni flow due to the surfactant concentration gradient. The presence of a Marangoni flow would stabilize the interface, leading to longer film drainage. The surface flow in the current experiments can be potentially dominated by either surface diffusion and advection. According to Yang *et al.*, the Pe for the interface can be defined as $\mathrm{Pe}_s = Uh/\varepsilon D_s$, where h is the film thickness, $\varepsilon = \frac{h}{\lambda}$ with λ the characteristic wavelength of the deformed thin film. $\mathrm{Pe}_s \sim 100 \gg 1$ in the current experiments, which indicates the advection is dominant over the surface diffusion. Eqn (1) indicates the relaxation of concentration gradients due to Marangoni convection *versus* that due to the surfactant diffusion. If $\mathrm{Ma} \ll 1$, the diffusion process is fast, and the surface concentration equilibrates before Marangoni flows can be established. Otherwise, if $\mathrm{Ma} \gg 1$, Marangoni flows are established before surfactant diffuses to interface. Despite the fact that there are glancing collisions between the droplets, the time scale for both the Marangoni flow and surface flow is $O(10^{-4})s$, which is much smaller than the time scale of rotation of the droplets $O(1)s$. Therefore, the surfactant distribution at droplet interface is dominated by the Marangoni flow and surface flow.

Here, the timescale it takes to establish the Marangoni flow is[65]

$$\tau_m = \frac{\mu R}{E_0} \tag{2}$$

where μ is the viscosity of the continuous phase, R is the average radius defined in the previous section, and E_0 is the Marangoni modulus. Based on Henry's isotherm, E_0 can be defined as $E_0 = R_{ig}T\Gamma_{eq}$, with R_{ig} as the ideal gas constant, T as the room temperature, and Γ_{eq} is the equilibrium surface concentration, which can be calculated using Langmuir isotherm $\Gamma_{eq} = \Gamma_\infty \kappa C/(1 + \kappa C)$. Eqn (2) indicates that a higher surface coverage leads to a larger Marangoni modulus, and thus lower τ_m, which implies that higher surfactant concentration (below CMC) induces stronger Marangoni flow in the current system. Alternatively, the droplet radius in eqn (2) can be replaced with thin film radius, $\tilde{r} \sim R(Ca)^{1/2}$ for $\mathrm{Ca} \ll 1$. The timescale for the surfactant bulk diffusion can be defined as[13]

$$\tau_D = \frac{(h_r^3 h_p)^{\frac{1}{2}}}{D} \tag{3}$$

Here, h_r is the depletion depth for the surfactant diffusion inside the droplet, h_p is the depletion depth for a plane surface and D is the surfactant diffusivity. Based on the mass balance of surfactant molecules in the subsurface and droplet interface according to Alvarez *et al.*,[13] depletion depth h_r for surfactant inside droplet can be obtained as[15]

$$h_r = r\left[1 - \left(1 - \frac{3h_p}{r}\right)^{1/3}\right] \tag{4}$$

where $h_p = \frac{\Gamma_{eq}}{C}$ and r is an independent variable that will be substituted by the droplet radius in the calculation. Here, Γ_{eq} is the equilibrium surface concentration, C is the bulk surfactant concentration. Note that eqn (4) expresses the depletion depth for a concave spherical interface, so the droplet radius must satisfy $r > 3h_p$ such that the depletion depth, h_r, is smaller than the droplet radius to provide sufficient surfactant molecules to the interface. The surfactant diffusivity, D, is extracted from the dynamic IFT measurement using the Ward and Tordai equation as discussed in the previous section. The interface between the two droplets flattens and a thin film forms when the droplets approach each other. Therefore, to ensure the appropriate usage of eqn (4) for a spherical droplet, the radius of the thin film needs to be checked. The thin film radius can be approximated as $\tilde{r} = r(Ca/\pi)^{1/2}$. In the current study, average droplet radius $r \approx 40$ μm, $Ca \sim O(10^{-3})$, and $\tilde{r} \sim O(10^{-1})$ μm $\ll r$. The thin film radius is much smaller than the droplet radius and can be neglected, which justifies the usage of eqn (4) in this study. Based on eqn (2)–(4), the Ma can be expressed as a function of the bulk surfactant concentration $C <$ CMC. When $C >$ CMC, particularly for Triton X-100, studies have shown that the effective diffusivity when micelles present in the bulk can be much greater than the diffusivity of the monomers and can increase with the increasing C.[59,66] An expression to obtain the effective diffusivity above CMC was previously presented by Joos and Hunsel[67] as,

$$D_{eff} = D\left(1 + \frac{C - \mathrm{CMC}}{\mathrm{CMC}}\right) \times \left(1 + \frac{C - \mathrm{CMC}}{\mathrm{CMC}}\frac{D_m}{D}\right) \tag{5}$$

where D_{eff} is the effective diffusivity and D_m is the diffusivity of the micelles. D_m/D can be assumed to be 0.25 according to the study by Horozov and Joos,[66] though this may be viewed as a simplifying approximation and would vary depending on the surfactant type. Eqn (5) can be used to evaluate the τ_D for Triton

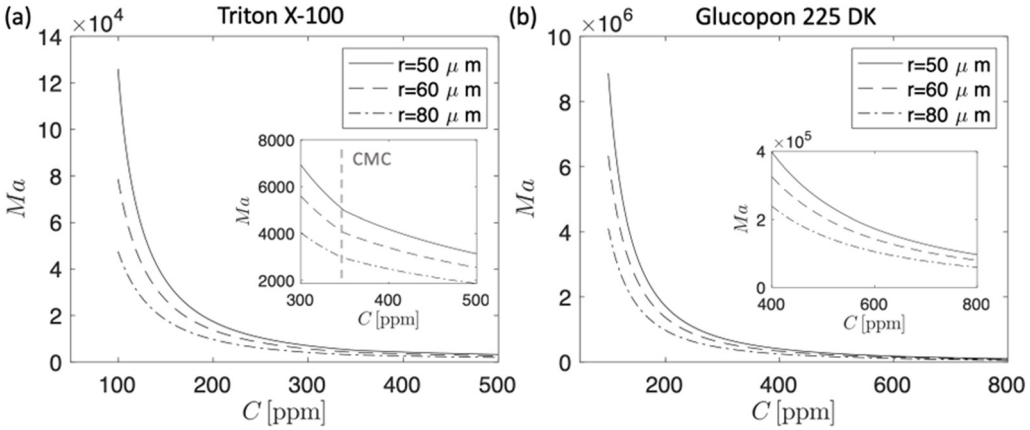

Fig. 10 Ma = τ_D/τ_m is plotted as a function of surfactant bulk concentration, C, for different droplet radius, r. Both surfactants, Triton X-100 (a) and Glucopon 225 DK (b), show that Ma decreases with increasing C, indicating that the time scale for the Marangoni flow to develop increases.

X-100 when concentration is above CMC. In addition to the impact of micelles on surfactant diffusivity, the depletion depth, h_r and h_p, has shown to be different due to the dissolution of the micelles.[68] However, according to the study by Liao *et al.*,[68] the dependence of the depletion depth on the dissolution of micelles is complicated, as the resultant depletion depth may become either smaller or greater if the micelles show a faster or slower dissolution rate, respectively. For the current study, therefore, the depletion depth is assumed to remain constant for C > CMC for simplicity.

Fig. 10 shows the values of Ma plotted as a function of surfactant bulk concentration, C, for both Triton X-100 and Glucopon 225 DK. The values of the surfactant properties in Fig. 10 are based on the characterization shown in Table 2. Within the current range of C, both surfactants show that the values of Ma are well above unity, suggesting that the Marangoni flow is already well established compared to the process of the surfactant's diffusion to the interface, resulting in a Marangoni stress that has a strong impact on film drainage. When C increases, Ma does decrease by about an order of 10^1 for both surfactants, which results in a significant reduction of 90% of Ma. Though Ma is still much greater than 1, the decreasing Ma as a function of C clearly shows that it takes less time for the surfactants to repopulate to the droplet interface *via* diffusion with increasing concentration and resultant decrease in diffusional depletion depth h_p and h_r (see Eqn (3)). While τ_m the denominator in eqn (1) decreases when E_0 increases due to the increase of Γ_{eq} from eqn (2), Ma still decreases, indicating that τ_D must decrease much faster than the decrease of τ_m. That is, the rate at which the surfactant molecules repopulate to the droplet interface relatively increases, and they tend to affect the Marangoni flow by eliminating the surfactant gradient along the interface. The diminished surfactant gradient certainly is possible to cause the Marangoni stress to be suppressed and thus the film drainage is enhanced. The trend of this Ma scale can help explain the decrease of the film drainage time from Fig. 8 when the surfactant molecules are inside the droplet (a reservoir of surfactants to draw from to re-populate the interface as surfactants are swept away), which also agrees well with previous theoretical studies.[21,23,26]

However, the calculated Ma only shows a monotonic decrease with increasing C, which still cannot explain the plateau of film drainage time above a certain concentration. According to the IFT measurement from Fig. 6, Triton X-100 reaches CMC at around 324 ppm, which is about the same concentration beyond which the film drainage time plateaus. Clearly, when concentration is above CMC, the solubility of the free surfactants in the bulk is reached, micelles form and surface coverage reaches its maximum value. In this case, τ_m becomes constant due to the saturation of surface coverage, while τ_d continues to decrease based on eqn (5), due to the impact of the micelles on the effective diffusivity, $D_{eff.}$,[69–71] which leads to a decreasing Ma above CMC. Similarly, for Glucopon 225DK, Ma keeps decreasing when the concentration is above 400 ppm. However, from the measurement of Fig. 6, the CMC of Glucopon 225 DK is close to 1000 ppm, which is much greater than the critical concentration at 400 ppm in Fig. 8(b) where the film drainage time plateaus. Similar trend has been observed in the foam film behavior[72] using Triton X100 that the film volume becomes constant at concentration of Triton X100 above CMC. This is consistent with our current situation that Marangoni flow and capillary stress no longer play a significant role in changing the film drainage due to the saturation of the Triton X100. This continuing decrease of Ma for both surfactants suggests that there must be other reasons that cause the plateau of the film drainage time with increasing concentration, explored next.

Marangoni *vs.* capillary effects: deformation of droplet interface

In addition to the surfactant bulk diffusion time scale, it is also important to compare the Marangoni stress to the capillary stress along the interface,[65,73] defined as

$$\mathrm{Ma}_\gamma = \frac{E_0}{\gamma_{eq}} \quad (6)$$

where $E_0 = R_{ig}T\Gamma_{eq}$ as defined in the previous section, to understand film drainage in coalescence. The equation of state for equilibrium IFT,[18] γ_{eq}, using the Langmuir isotherm is

$$\gamma_{eq} = \gamma_0 + nR_{ig}T\Gamma_\infty \ln\left(1 - \frac{\kappa C}{1+\kappa C}\right) \quad (7)$$

where γ_0 is the surfactant-free IFT, and $n = 1$ for non-ionic surfactant. Γ_∞ and κ is the maximum surface coverage and equilibrium constant, as listed in Table 2.

For both surfactants as shown in Fig. 11(a) and (b), the values of Ma_γ monotonically increase above 1 with increasing surfactant concentration. For TritonX-100, however, the surfactant reaches CMC around 350 ppm such that $\Gamma \to \Gamma_\infty$ and γ_{eq} becomes constant. Therefore, the calculated Ma_γ also remains unchanged when $C > 350$ ppm for Triton X-100. This constant Ma_γ can also contribute to the explanation of the plateau of the film drainage time. Within the current range of surfactant concentration, a critical concentration can be extracted at which $Ma_\gamma \sim 1$. There can be two complementary viewpoints on the physical interpretation of this Ma effect on film drainage.

Without surfactants present, it is well understood that droplets with a higher interfacial tension coalesce more rapidly than those with lower values, due to the thermodynamic favorability of reducing the surface-to-volume ratio of the system. According to the study by Dai & Leal,[31] the magnitude of Ma_γ indicates the impact of Marangoni stress *versus* the capillary stress. From eqn (6), a large γ_{eq} enhances coalescence between the two droplets (Ma_γ small), while a small γ_{eq} inhibits coalescence (Ma_γ large). The trend of the Ma_γ can explain, particularly for Glucopon 225, the previously unexplainable observation that film drainage time is no longer decreasing when the concentration is increased above a certain value, due to the lowered γ_{eq} (balancing the re-population effect). Similar non-monotonic trend has been observed in Rao *et al.*[74] and Bhamla *et al.*,[75] both of which have emphasized the significant impact of Marangoni stress on the film drainage induced by variation of surfactant concentration below or approaching CMC.

The second viewpoint, particularly useful when surfactants are present is that the larger Ma_γ suggests stronger Marangoni stress (induced by the Marangoni flow), which can induce strong deformation of the two droplets. In particular, according to Dai & Leal, a dimpled configuration of the thin film occurs, with the Ca in the order of $O(10^{-3})$, such that the thickness at the rim of the thin film becomes smaller than that at the center of the thin film. Based on Ramachandran & Leal,[76] the equation we can use to predict film drainage time under dimpled film region is $t_d G \sim \frac{1}{\alpha} Ca^{\frac{17}{12}} \left(A^*_{H,eff}\right)^{-\frac{1}{6}}$, where $\alpha = \frac{\alpha'\mu}{R}$ is dimensionless slip coefficient, α' is the dimensional slip coefficient, μ is the viscosity of the continuous phase, and $A^*_{H,eff} = \frac{A_{H,eff}}{\gamma R^2}$ is dimensionless Hamaker constant. Based on the work from Ramachandran & Leal[76] and Ivanova-Stancheva,[77] we can estimate both constants to be $\alpha \sim 2 \times 10^{-5}$ and $A^*_{H,eff} \sim 3 \times 10^{-10}$. With $Ca \sim 10^{-3}$, $R \sim 40$ μm, and $G \sim 20\ s^{-1}$. The predicted $t_d \sim 5s$ using the above equation based on the condition in our current systems. Though the predicted drainage time is slightly higher than the film drainage time measured in our experiments $t_{d\_exp} \sim O(1)s$, the measured values are close to the prediction, which further provides evidence that the film is indeed dimpled in the current experiments. The dimpled thin film will significantly inhibit the film drainage as compared to a flat thin film and increase the drainage time. Despite the fact that increased Marangoni stress reduces the mobility of the interface, according to the study by Dai & Leal,[31] the dimpled film is responsible for a significant portion of the reduced film drainage rate. Note that the *Ca* and γ_{eq} used in the current work are similar to the parameters used for the computation of droplet deformation shape by Dai & Leal. While the film drainage itself may be slower with a dimpled configuration, the process of rupture could be much faster with dimpling, if present. Overall, these two aforementioned phenomena can explain the large variation of the film drainage time measured when the surfactant is increased above critical concentration. However, it is not clear that from the scaling relationship with Ca shown in Fig. S7, SI that dimpling is occurring, so, in addition to the above two viewpoints, it is also likely that the steric interactions could potentially induce repulsive forces at

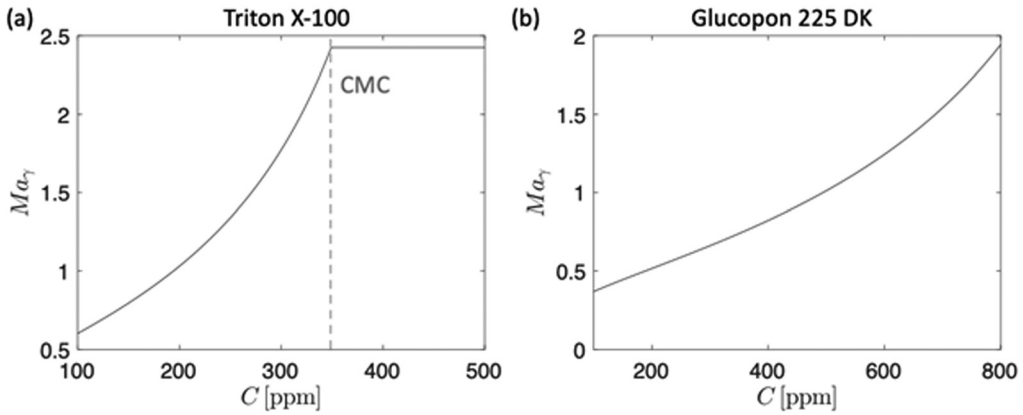

Fig. 11 $Ma_\gamma = E_0/\gamma_{eq}$ is plotted as a function of surfactant bulk concentration, *C*. Both surfactants, Triton X-100 (a) and Glucopon 225 DK (b), show that Ma increases with increasing *C*, indicating that the Marangoni stress becomes stronger than the capillary stress at the interface.

the interface especially when the interfaces reach the point near rupture (<100 nm). This repulsive force can be induced by the osmotic pressure when there is overlapped region of surfactants on two approaching droplets or there is a decrease in the volume of the surfactant molecules at the droplet interface for two touched droplets. In the current experiments, all coalescences are observed with the rotation angle below 45°. However, experimental results from Narayan *et al.* have also shown that coalescence can be observed at rotation angles above 45°, suggesting coalescence can also occur during separation phase as well.

Impact of velocity and size of the droplets

Finally, it should be noted that in addition to the viscosity ratio and surfactant concentration, the incident velocity and size of the droplet can also vary in the experiment and affect the drainage time. Experimentally, both velocity and drop size are easily varied. For instance, the velocity of the droplets will change if the pressure from the continuous phase changes during the trapping. In addition, the size of the droplets is strongly dependent on the ratio of the pressure between the continuous phase and dispersive phase flow at the T-junction. Seminal works[25] have shown that both the velocity and size of the droplets will have a significant impact on the droplet coalescence, as the different resultant hydrodynamic conditions can affect the film drainage behavior. In particular, study[78] has shown that the shape of the droplets, whether spherical or deformed depending on their sizes will affect the film shape leading to variation of drainage time. For possible impact of the droplet velocity and size on the film drainage times, see the results in Fig. 8 plotted based on droplet velocity, radius, and strain rate in Fig. S4–S6, along with a brief discussion.

Conclusion

In the present work, the impact of viscosity ratio and surfactant concentration on droplet stability was investigated. In particular, the droplet stability was visualized *via* the coalescence of the droplet and quantitatively measured *via* the film drainage time between the two approaching droplets. First, systems with different viscosity ratios, λ, between the droplet phase and continuous phase were performed using a 6-channel microfluidic device, with droplets trapped at the cross-slot of the channels. The experiments show that droplet coalescence was observed for systems with $\lambda < 1$, but no coalescence when $\lambda > 1$ even without adding surfactants in the system. The results of λ dependent coalescence agree well with the seminal theoretical study that $\lambda > 1$ induces greater viscous stress at the droplet interface that will inhibit the film drainage and droplet coalescence. For those systems with $\lambda < 1$, however, coalescence is not observed when the surfactant is added to the continuous phase beyond a certain value, suggesting a lowered interfacial tension that inhibits the droplet coalescence.

Second, experiments with surfactant inside the droplets were also performed and the film drainage time was quantified with the surfactant concentration. Prior work by Narayan *et al.* showed an increased film drainage time with increased surfactant concentration in the continuous phase. Now, by placing the surfactant in the dispersed droplet phase, the film drainage time was found to decrease or plateau as the surfactant concentration approached a critical concentration.

To explain the new observation of decreasing film drainage time *versus* surfactant inside the droplet, the Marangoni number, Ma, has been calculated based on various definition that indicates different physical meanings. First, when Ma is defined as the ratio between the surfactant diffusion time scale *versus* the Marangoni flow time scale, the values are much greater than 1 for both Triton X-100 and Glucopon 225DK. The large values of Ma suggest that the Marangoni flow occurs before the surfactant molecules diffuse and adsorbed onto the interface. However, when the concentration of both surfactants increases approaching CMC, Ma decreases by 1 order of magnitude, suggesting that it starts taking relatively less time for the surfactant molecules to transport to the interface. This reduced diffusion time scale can explain the suppressed Marangoni stress at the droplet interface, and therefore, the reduced film drainage time at low concentrations.

A second definition of Ma_γ is defined as the ratio between the Marangoni stress and capillary stress. For both surfactants, Ma_γ increases when surfactant concentration is increasing below CMC, suggesting that the Marangoni becomes more significant over the Capillary stress. A larger Ma_γ induces a stronger interfacial deformation that can inhibit the film drainage time and trigger the film rupture, which leads to a large variation in the film drainage time. These effects help explain the change in film drainage time behavior at higher surfactant concentrations.

Overall, the current work provides insight into the fundamental understanding of the impact of viscosity ratio and surfactant concentration on the film drainage time between the droplets and droplet coalescence, particularly in the presence of soluble surfactants. The results can inform the emulsion stability based on the liquid–liquid systems in various situations such as the bilgewater and the aqueous film forming foam. Knowing the droplet stability based on the surfactant concentration used in the system can help improve the mitigation strategies of oil separation from the bulk aqueous phase. For instance, the residence times during the operation can be informed to provide guidance towards the development of the optimal treatment methods. Since the current study only focuses on the surfactant concentration below CMC, a future study could increase the surfactant concentration above CMC and investigate the impact of micelles on the film drainage time. In addition, the diesel oil involved in the bilgewater or AFFF applications is usually a complex fluid that can include surface active additives. Future studies can also incorporate the additives together with the surfactants in the systems to further bridge the model system and the real systems. Lastly, a systematic study of a wider range of droplet sizes and flow conditions for future work can expand the current understanding of droplet stability towards a broader scope of applications such as food processing or cosmetic manufacturing.

Conflicts of interest

There are no conflicts of interest to declare.

Data availability

The data supporting this article have been included as part of the SI, which contains figures and tables with detailed representation of the data presented in this paper. See DOI: **https://doi.org/10.1039/d4sm00644e**

Acknowledgements

This work is performed under the support of the DOD Strategic Environmental Research and Development Program (SERDP) project WP19-1407. Portion of this work were conducted at the Minnesota Nano Center, which is supported by the National Science Foundation through the National Nano Coordinated Infrastructure Network (NNCI) under number ECCS-1542202. The authors would like to thank Shihao Liu for helping with the surfactant characterization programming code.

References

1 J. Church, D. M. Paynter and W. H. Lee, In Situ Characterization of Oil-in-Water Emulsions Stabilized by Surfactant and Salt Using Microsensors, *Langmuir*, 2017, **33**, 9731–9739.
2 J. Church, *et al.*, Identification and characterization of bilgewater emulsions, *Sci. Total Environ.*, 2019, **691**, 981–995.
3 Y. Chen, S. Narayan and C. S. Dutcher, Phase-Dependent Surfactant Transport on the Microscale: Interfacial Tension and Droplet Coalescence, *Langmuir*, 2020, **36**, 14904–14923.
4 J. Church, *et al.*, Impact of Interfacial Tension and Critical Micelle Concentration on Bilgewater Oil Separation, *J. Water Process Eng.*, 2021, **39**, 101684.
5 H. Eskandarloo, M. J. Selig and A. Abbaspourrad, In situ H_2O_2 generation for de-emulsification of fine stable bilge water emulsions, *Chem. Eng. J.*, 2018, **335**, 434–442.
6 S. Narayan, D. B. Moravec, B. G. Hauser, A. J. Dallas and C. S. Dutcher, Removing Water from Diesel Fuel: Understanding the Impact of Droplet Size on Dynamic Interfacial Tension of Water-in-Fuel Emulsions, *Energy Fuels*, 2018, **32**, 7326–7337.
7 C. Stanfel, Fuel filtration: Protecting the diesel engine, *Filtr. Sep.*, 2009, **46**, 22–25.
8 K. Hinnant, M. Button, S. Giles, A. Snow and R. Ananth, Fuel effects on aqueous film formation and foam degradation and their impact on fire suppression by foams containing fluorosurfactants, *Fire Mater.*, 2020, 1–9, DOI: **10.1002/fam.2916**.
9 K. M. Hinnant, S. L. Giles, E. P. Smith, A. W. Snow and R. Ananth, Characterizing the Role of Fluorocarbon and Hydrocarbon Surfactants in Firefighting-Foam Formulations for Fire-Suppression, *Fire Technol.*, 2020, **56**, 1413–1441.
10 A. Sontake and M. Wagh, S. The Phase-out of Perfluorooctane Sulfonate (PFOS) and the Global Future of Aqueous Film Forming Foam (AFFF), Innovations in Fire Fighting Foam, *Chem. Eng. Sci.*, 2014, **2**, 11–14.
11 L. Ahrens, Polyfluoroalkyl compounds in the aquatic environment: A review of their occurrence and fate, *J. Environ. Monit.*, 2011, **13**, 20–31.
12 Q. Brosseau, J. Vrignon and J.-C. Baret, Microfluidic Dynamic Interfacial Tensiometry (μDIT), *Soft Matter*, 2014, **10**, 3066–3076.
13 N. J. Alvarez, L. M. Walker and S. L. Anna, Diffusion-limited adsorption to a spherical geometry: The impact of curvature and competitive time scales, *Phys. Rev. E*, 2010, **82**, 11604.
14 N. J. Alvarez, *An Experimental and Theoretical Study of Surfactant Dynamics at Microscale Interfaces*, Carnegie Mellon University, 2011, DOI: **10.1184/R1/6714704.V1**.
15 F. Jin, R. Balasubramaniam and K. J. Stebe, Surfactant Adsorption to Spherical Particles: The Intrinsic Length Scale Governing the Shift from Diffusion to Kinetic-controlled Mass Transfer, *J. Adhes.*, 2004, **80**, 773–796.
16 N. J. Alvarez, L. M. Walker and S. L. Anna, A Microtensiometer To Probe the Effect of Radius of Curvature on Surfactant Transport to a Spherical Interface, *Langmuir*, 2010, **26**, 13310–13319.
17 N. J. Alvarez, D. R. Vogus, L. M. Walker and S. L. Anna, Using bulk convection in a microtensiometer to approach kinetic-limited surfactant dynamics at fluid–fluid interfaces, *J. Colloid Interface Sci.*, 2012, **372**, 183–191.
18 Y. Chen and C. S. Dutcher, Size dependent droplet interfacial tension and surfactant transport in liquid-liquid systems, with applications in shipboard oily bilgewater emulsions, *Soft Matter*, 2020, **16**(12), 2994–3004.
19 X. Li, R. Shaw, G. M. Evans and P. Stevenson, A simple numerical solution to the Ward-Tordai equation for the adsorption of non-ionic surfactants, *Comput. Chem. Eng.*, 2010, **34**, 146–153.
20 T. Kairaliyeva, *et al.*, Surface Tension and Adsorption Studies by Drop Profile Analysis Tensiometry, *J. Surfactants Deterg.*, 2017, **20**, 1225–1241.
21 D. Langevin, Coalescence in foams and emulsions: Similarities and differences, *Curr. Opin. Colloid Interface Sci.*, 2019, **44**, 23–31.
22 I. B. Ivanov and T. T. Traykov, Hydrodynamics of thin liquid films. Rate of thinning of emulsion films from pure liquids, *Int. J. Multiphase Flow*, 1976, **2**, 397–410.
23 I. B. Bazhlekov, A. K. Chesters and F. N. Van De Vosse, The effect of the dispersed to continuous-phase viscosity ratio on film drainage between interacting drops, *Int. J. Multiphase Flow*, 2000, **26**, 445–466.
24 L. G. Leal, Flow induced coalescence of drops in a viscous fluid, *Phys. Fluids*, 2004, **16**, 1833–1851.
25 S. Narayan, *et al.*, Insights into the microscale coalescence behavior of surfactant-stabilized droplets using a microfluidic hydrodynamic trap, *Langmuir*, 2020, **36**, 9827–9842.
26 A. K. Chesters, Modelling of coalescence processes in fluid-liquid dispersions. A review of current understanding, *Chem. Eng. Res. Des.*, 1991, **69**, 259–270.
27 Y. T. Hu, D. J. Pine and L. G. Leal, Drop deformation, breakup, and coalescence with compatibilizer, *Phys. Fluids*, 2000, **12**, 484–489.
28 H. Yang, C. C. Park, Y. T. Hu and L. G. Leal, The coalescene of two equal-sized drops in a two-dimensional linear flow, *Phys. Fluids*, 2001, **13**, 1087–1106.

29 J. W. Ha, Y. Yoon and L. G. Leal, The effect of compatibilizer on the coalescene of two drops in flow, *Phys. Fluids*, 2003, **15**, 849–867.
30 A. S. Hsu, A. Roy and L. G. Leal, Drop-size effects on coalescence of two equal-sized drops in a head-on collision, *J. Rheol.*, 2008, **52**, 1291–1310.
31 B. Dai and L. G. Leal, The mechanism of surfactant effects on drop coalescence, *Phys. Fluids*, 2008, **20**, 040802.
32 Y. Yoon, M. Borrell, C. C. Park and L. G. Leal, Viscosity ratio effects on the coalescence of two equal-sized drops in a two-dimensional linear flow, *J. Fluid Mech.*, 2005, **525**, 355–379.
33 I. B. Ivanov, K. D. Danov and P. A. Kralchevsky, Flocculation and coalescence of micron-size emulsion droplets, *Colloids and Surfaces A: Physicochemical and Engineering Aspects*, Elsevier Science Publishers B.V., 1999, vol. 152, pp. 161–182.
34 E. Chatzigiannakis, P. Veenstra, D. Ten Bosch and J. Vermant, Mimicking coalescence using a pressure-controlled dynamic thin film balance, *Soft Matter.*, 2020, **16**, 9410–9422, DOI: **10.1039/d0sm00784f**.
35 E. Chatzigiannakis and J. Vermant, Breakup of Thin Liquid Films: From Stochastic to Deterministic, *Phys. Rev. Lett.*, 2020, **125**, 158001.
36 D. Kumar, *A Microfluidic Device for Producing Controlled Collisions Between Two Soft Particles*, 2016.
37 M. Roché, M. Aytouna, D. Bonn and H. Kellay, Effect of surface tension variations on the pinch-Off behavior of small fluid drops in the presence of surfactants, *Phys. Rev. Lett.*, 2009, **103**, 264501.
38 J. Qi, Z. L. Yu, G. P. Liao, Z. Y. Luo and B. F. Bai, Effect of nanoparticle surfactants on droplet formation in a flow-focusing microchannel, *Phys. Fluids*, 2021, **33**, 112008.
39 X. Shang, Z. Luo, B. Bai and G. Hu, A front-tracking method for simulating interfacial flows with particles and soluble surfactants, *J. Comput. Phys.*, 2023, **493**, 112476.
40 Z. Y. Luo, X. L. Shang and B. F. Bai, Marangoni effect on the motion of a droplet covered with insoluble surfactant in a square microchannel, *Phys. Fluids*, 2018, **30**, 077101.
41 Z. Y. Luo, X. L. Shang and B. F. Bai, Effect of soluble surfactant on the motion of a confined droplet in a square microchannel, *Phys. Fluids*, 2019, **31**, 117104.
42 E. Lac, A. Morel and D. Barthès-biesel, Hydrodynamic interaction between two identical capsules in simple shear flow, *J. Fluid Mech.*, 2007, **573**, 149–169.
43 W. Wei, Z. Luo and B. Bai, Hydrodynamic interaction of two droplets covered with insoluble surfactant in shear flow, *Int. J. Multiphase Flow*, 2024, **170**, 104646.
44 A. Shenoy, D. Kumar, S. Hilgenfeldt and C. M. Schroeder, Flow Topology during Multiplexed Particle Manipulation Using a Stokes Trap, *Phys. Rev. Appl.*, 2019, **12**, 054010.
45 D. Kumar, A. Shenoy, S. Li and C. M. Schroeder, Orientation control and nonlinear trajectory tracking of colloidal particles using microfluidics, *Phys. Rev. Fluids*, 2019, **4**, 114203.
46 A. Shenoy, C. V. Rao and C. M. Schroeder, Stokes trap for multiplexed particle manipulation and assembly using fluidics, *Proc. Natl. Acad. Sci. U. S. A.*, 2016, **113**, 3976–3981.
47 J. Crocker and D. Grier, Methods of Digital Video Microscopy for Colloidal Studies | Elsevier Enhanced Reader, *J. Colloid Interface Sci.*, 1995, **179**, 298–310.
48 A. V. Rawlings and K. J. Lombard, A review on the extensive skin benefits of mineral oil, *Int. J. Cosmet Sci.*, 2012, **34**, 511–518.
49 J. F. Nash, S. D. Gettings, W. Diembeck, M. Chudowski and A. L. Kraus, A toxicological review of topical exposure to white mineral oils, *Food Chem. Toxicol.*, 1996, **34**, 213–225.
50 S. Narayan, *et al.*, Dilatational rheology of water-in-diesel fuel interfaces: Effect of surfactant concentration and bulk-to-interface exchange, *Soft Matter*, 2021, **17**, 4751–4765.
51 A. V. Pietrini and P. L. Luisi, Cell-free protein synthesis through solubilisate exchange in water/oil emulsion compartments, *ChemBioChem*, 2004, **5**, 1055–1062.
52 M. Nakano, *et al.*, Single-molecule PCR using water-in-oil emulsion, *J. Biotechnol.*, 2003, **102**, 117–124.
53 K. R. Pandit, P. E. Rueger, R. V. Calabrese, S. R. Raghavan and I. M. White, Assessment of surfactants for efficient droplet PCR in mineral oil using the pendant drop technique, *Colloids Surf., B*, 2015, **126**, 489–495.
54 A. Jalili, M. Bagheri, A. Shamloo and A. H. Kazemipour Ashkezari, A plasmonic gold nanofilm-based microfluidic chip for rapid and inexpensive droplet-based photonic PCR, *Sci. Rep.*, 2021, **11**, 1–13.
55 P. S. Chae, M. J. Wander, K. H. Cho, P. D. Laible and S. H. Gellman, Carbohydrate-containing Triton X-100 analogues for membrane protein solubilization and stabilization, *Mol. BioSyst.*, 2013, **9**, 626–629.
56 R. Ananth, A. Snow, K. Hinnant, S. Giles and J. Farley, *Final Report Fluorine-Free Foams with Oleophobic Surfactants and Additives for Effective Pool Fire Suppression*. (2021).
57 R. Ananth, A. W. Snow, K. M. Hinnant, S. L. Giles and J. P. Farley, Synergisms between siloxane-polyoxyethylene and alkyl polyglycoside surfactants in foam stability and pool fire extinction, *Colloids Surf., A*, 2019, **579**, 123686.
58 C. Dong, C.-T. Hsu, C.-Y. Chiu and S.-Y. Lin, A Study on Surfactant Adsorption Kinetics: Effect of Bulk Concentration on the Limiting Adsorption Rate Constant, *Langmuir*, 2000, **16**, 4573–4580.
59 J. Eastoe and J. S. Dalton, Dynamic surface tension and adsorption mechanisms of surfactants at the air-water interface, *Adv. Colloid Interface Sci.*, 2000, **85**, 103–144, DOI: **10.1016/S0001-8686(99)00017-2**.
60 F. D. Rumscheidt and S. G. Mason, Particle motions in sheared suspensions XI. Internal circulation in fluid droplets (experimental), *J. Colloid Sci.*, 1961, **16**, 210–237.
61 Z. Wang, Q. Dong, Y. Zhang, J. Wang and J. Wen, Numerical study on deformation and interior flow of a droplet suspended in viscous liquid under steady electric fields, *Adv. Mech. Eng.*, 2014, **2014**, 532797.
62 B. Dai and L. G. Leal, The mechanism of surfactant effects on drop coalescence, *Phys. Fluids*, 2008, **20**, 040802.
63 K. J. Stebe, S.-Y. Lin and C. Maldarelli, Remobilizing surfactant retarded fluid particle interfaces. I. Stress-free conditions at the interfaces of micellar solutions of surfactants with fast sorption kinetics, *Phys. Fluids*, 1991, **3**, 010003.

64 M. R. King and D. T. Leighton, Measurement of shear-induced dispersion in a dilute emulsion, *Phys. Fluids*, 2001, **13**, 397–408.
65 H. Manikantan and T. M. Squires, Surfactant dynamics: Hidden variables controlling fluid flows, *J. Fluid Mech.*, 2020, **892**, 1–115.
66 T. Horozov and P. Joos, Dynamic Surface Tension of Surfactant Solutions Studied by Peaktensiometry, *J. Colloid Interface Sci.*, 1995, **173**, 334–342, DOI: **10.1006/jcis.1995.1333**.
67 P. Joos and J. Van Hunsel, Adsorption kinetics of micellar Brij 58 solutions, *Colloids Surf.*, 1988, **33**, 99–108.
68 Y. C. Liao and O. A. Basaran, & Franses, E. I. Micellar Dissolution and Diffusion Effects on Adsorption Dynamics of Surfactants, *AIChE J.*, 2003, **49**, 3229–3240.
69 K. D. Danov, P. A. Kralchevsky, N. D. Denkov, K. P. Ananthapadmanabhan and A. Lips, Mass transport in micellar surfactant solutions: 1. Relaxation of micelle concentration, aggregation number and polydispersity, *Adv. Colloid Interface Sci.*, 2006, **119**, 1–16.
70 K. D. Danov, P. A. Kralchevsky, N. D. Denkov, K. P. Ananthapadmanabhan and A. Lips, Mass transport in micellar surfactant solutions: 2. Theoretical modeling of adsorption at a quiescent interface, *Adv. Colloid Interface Sci.*, 2006, **119**, 17–33.
71 K. D. Danov, D. S. Valkovska and P. A. Kralchevsky, Adsorption relaxation for nonionic surfactants under mixed barrier-diffusion and micellization-diffusion control, *J. Colloid Interface Sci.*, 2002, **251**, 18–25.
72 J. M. Frostad, D. Tammaro, L. Santollani, S. Bochner de Araujo and G. G. Fuller, Dynamic fluid-film interferometry as a predictor of bulk foam properties, *Soft Matter*, 2016, **12**, 9266–9279.
73 D. Quéré, Fluid coating on a fiber, *Annu. Rev. Fluid Mech.*, 1999, **31**, 347–384.
74 A. A. Rao, D. T. Wasan and E. D. Manev, Foam stability---effect of surfactant composition on the drainage of microscopic aqueous films, *Chem. Eng. Commun.*, 1982, **15**, 63–81.
75 M. Saad Bhamla, C. Chai, M. A. Àlvarez-Valenzuela, J. Tajuelo and G. G. Fuller, Interfacial mechanisms for stability of surfactant-laden films, *PLoS One*, 2017, **12**, 0175753.
76 A. Ramachandran and L. G. Leal, Effect of interfacial slip on the thin film drainage time for two equal-sized, surfactant-free drops undergoing a head-on collision: A scaling analysis, *Phys. Rev. Fluids*, 2016, **1**, 1–17.
77 D. Ivanova-Stancheva, Influence of the Hamaker constant on the value of the critical thickness of foam films, *Coatings*, 2019, **9**, 576.
78 I. B. Ivanov, K. D. Danov and P. A. Kralchevsky, Flocculation and coalescence of micron-size emulsion droplets. *Colloids and Surfaces A: Physicochemical and Engineering Aspects*, Elsevier Science Publishers B.V., 1999, vol. 152, pp. 161–182.